Journal of Energy Chemistry 106 (2025) 600–607

Contents lists available at ScienceDirect

Journal of Energy Chemistry

journal homepage: www.elsevier.com/locate/jechem

http://www.journals.elsevier.com/journal-of-energy-chemistry/

CO_2-enhanced alkane aromatization over Cu-ZSM-5 zeolite: Insights into active sites and catalytic performance

Gaili Fan [a,b], Rongsheng Liu [b], Yang Zhao [c], Enze Chen [b], Siyang Yan [d], Jingfeng Han [b], Jiaxu Liu [d,*], Zhengxi Yu [b,*], Zhongmin Liu [b,*]

[a] School of Chemistry, Dalian University of Technology, Dalian 116024, Liaoning, China
[b] National Engineering Research Center of Lower-Carbon Catalysis Technology, Dalian National Laboratory for Clean Energy, Dalian Institute of Chemical Physics, Chinese Academy of Sciences, Dalian 116023, Liaoning, China
[c] Dalian National Laboratory for Clean Energy, Dalian Institute of Chemical Physics, Chinese Academy of Sciences, Dalian 116023, Liaoning, China
[d] State Key Laboratory of Fine Chemicals, Frontier Science Center for Smart Materials, School of Chemical Engineering, Dalian University of Technology, Dalian 116024, Liaoning, China

ARTICLE INFO

Article history:
Received 20 January 2025
Revised 28 February 2025
Accepted 28 February 2025
Available online 15 March 2025

Keywords:
Cu-ZSM-5
Aromatization
CO_2
Cu active centers
Cyclohexane

ABSTRACT

Aromatization of alkanes represents an important process in the chemical industry, traditionally relying on noble metal catalysts. Developing a non-noble metal catalyst and a relevant new process offers significant potential for promoting technologic progress in this field. Herein, we present Cu-ZSM-5 zeolite as a highly effective catalyst for alkane aromatization, achieving outstanding aromatics selectivity. In-situ Fourier transform infrared spectra of adsorbed nitric oxide, high-angle annular dark field scanning transmission electron microscopy, X-ray absorption spectroscopy, and electron paramagnetic resonance analyses reveal that the Cu^{2+} species act as the primary active centers for aromatics formation. During aromatization of alkanes, the reduction of Cu^{2+} to Cu^{+} species correlates with diminished aromatics selectivity. Notably, introducing CO_2 into the reaction feed not only enhances aromatics selectivity by maintaining Cu^{2+} species in their active oxidation state under reducing conditions, but also improves catalytic stability by eliminating coke. Furthermore, CO_2 is converted into CO and aromatic products during the reaction, offering a novel way for CO_2 utilization through the coupling reaction of alkane and CO_2.

1. Introduction

Aromatics, specifically benzene, toluene, and xylenes (BTX), serve as key indicators in the petrochemical industry and are extensively utilized as intermediate materials within the chemical sectors [1]. These compounds can play pivotal roles as basic raw materials for producing synthetic fibers, synthetic resins, synthetic rubbers, and fine chemicals such as dyes and pesticides [2]. Currently, catalytic reforming and steam cracking of naphtha are the primary sources of BTX production [3]. However, producing BTX from alkanes holds great potential to address the limitations of catalytic reforming, including high cost, high content of heavy aromatics, and high energy consumption [4]. The alkane aromatization reaction mainly involves three steps: the initial production of olefins via dehydrogenation or cracking, followed by the generation of olefins with long carbon chains, and then the formation of aromatics through cyclization and hydrogen transfer [5,6].

The essence of alkane aromatization technology lies in catalyst development, as alkanes would otherwise undergo thermal cracking at elevated temperatures in the absence of catalysts. The main direction for technological innovation is to find a non-noble catalyst to replace the traditional Pt/Al_2O_3 aromatization catalyst and to develop a relevant technology process. As zeolite was found to be effective for the alkane aromatization reaction through carbonium and hydrogen transfer mechanism [7], the catalytic performance of H-ZSM-5 zeolite in alkane conversion has been widely explored, attributed to its unique channel size (0.55 nm) and acidic properties for higher aromatics selectivity [8,9]. The coupling of dehydrogenation function with basic catalysis was expected to further enhance aromatics, which has been demonstrated by the introduction of metal cations such as Zn into the channels of H-ZSM-5 [10–13]. However, the loss of Zn active species in Zn/ZSM-5 at elevated temperatures limits its practical applications [14,15]. Copper, a classic component of many catalysts, has exhibited unique activity

* Corresponding authors.
E-mail addresses: liujiaxu@dlut.edu.cn (J. Liu), zhengxiyu@dicp.ac.cn (Z. Yu), liuzm@dicp.ac.cn (Z. Liu).

https://doi.org/10.1016/j.jechem.2025.02.048
2095-4956/

in various reactions, including CO_2 hydrogenation, methanol synthesis, and biomass hydro-deoxygenation [16–19]. However, copper catalysts are typically employed at lower temperatures due to the instability of their redox states at elevated temperatures [20,21].

A frequently observed phenomenon during the activation of copper-exchanged zeolites is auto-reduction, where certain Cu^{2+} species spontaneously transform to Cu^{+} at elevated temperatures in an inert environment, without a reducing agent [22–27]. Researchers have determined that the oxidation state of Cu in Cu-ZSM-5 zeolites depends on the evacuation temperature, with Cu^{+} species initially emerging at 473 K and progressively increasing until 873 K [28,29]. Giamello et al. reported that after heating at 873 K, Cu^{+} constitutes 70% of the total Cu in Cu-ZSM-5 [30]. A few examples of copper valence state change have been documented in the literature. Bokhoven et al. proposed a method for converting methane into methanol on Cu-MOR zeolite via partial oxidation with water, where methane is oxidized at Cu^{2+} oxide active centers, followed by Cu^{+} reoxidation to Cu^{2+} by water [31]. During thermal treatment in an NO/O_2 mixture, metallic Cu^{0} nanoparticles in Cu agglomerates on silica xerogels are oxidized to Cu^{+}/Cu^{2+} [32,33]. Some critical questions related to Cu-zeolite catalyst for aromatization reaction should be considered. (1) Can Cu-zeolite be an effective catalyst at high temperature? (2) Which state of Cu (Cu^{2+} or Cu^{+}) is more effective for the reaction? (3) if Cu^{2+} is more active, how does Cu keep in an oxidative state in the hydrocarbon reduction condition? The objective of this study is to answer these questions and further explore whether CO_2 can assist the Cu-zeolites in catalyzing alkane conversion reactions to yield aromatics.

Cu-ZSM-5 zeolite was employed as a catalyst for the conversion reaction of cyclohexane to aromatics. The results revealed that Cu-ZSM-5 zeolite exhibits excellent aromatization properties during the reaction, with Cu^{2+} species identified as the more active species in the aromatization pathway. In-situ experiments have demonstrated that the Cu^{2+} active species are converted into inactive Cu^{+}, accompanied by aromatics formation. The introduction of CO_2 to the cyclohexane feed could enhance the aromatics selectivity and prolong the reaction lifetime, attributed to the stabilization of the Cu^{2+} oxidation state, and the CO_2 is concurrently converted to CO and aromatics during the reaction.

Oxidation of copper supported on zeolites by CO_2 has not been previously reported despite CO_2 also revealing weak oxidizing properties. The climate change, driven by rising carbon dioxide (CO_2) levels, has emerged as a global problem, attracting worldwide attention to CO_2 utilization [34,35]. Our research also provides an innovative strategy for CO_2 utilization via the coupling reaction of alkanes and CO_2.

2. Experimental

2.1. Materials and reagents

H-ZSM-5 zeolite was purchased from Nankai University Catalyst Co., Ltd, which possesses a Si/Al ratio of 17. Cu $(NO_3)_2{\cdot}3H_2O$ and $NaNO_3$ were acquired from Damao Chemical Reagent Factory. Hexamethylene and *n*-hexane were bought from Guangdong Guanghua Sci-Tech Co., Ltd. CO_2 (CO_2, 85.0%; Ar, 15.0%) and helium (99.999%) were provided by Dalian Special Gas Co., Ltd. All chemicals were used as received without further purification.

2.2. Synthesis of Cu-ZSM-5 and Na-ZSM-5

Cu-ZSM-5 catalysts were synthesized by an ion-exchanged method. Firstly, three portions of 50 g H-ZSM-5 zeolite were individually placed into three beakers containing 500 g deionized water. Following that, 6.04 g Cu $(NO_3)_2{\cdot}3H_2O$ was weighed into the first beaker and stirred at room temperature for 30 min. In the second beaker, 12.08 g Cu $(NO_3)_2{\cdot}3H_2O$ was added and heated with stirring using 80 °C water bath for 3.5 h. 89.6 g Cu $(NO_3)_2{\cdot}3H_2O$ was placed into the third beaker and stirred in a 90 °C water bath for 2.5 h. Afterward, the three samples were filtered, washed with a large excess of water, dried at 130 °C for 4 h, and then calcined at 550 °C for 6 h. The samples are respectively named Cu0.9-ZSM-5, Cu1.9-ZSM-5, and Cu2.4-ZSM-5, where the numbers represent the mass percentages of Cu, which were characterized by an X-ray fluorescence spectrometer (XRF).

Na-ZSM-5 samples were also prepared by ion exchange method. Three beakers were first prepared, each containing 10 g H-ZSM-5 molecular sieve and 100 g deionized water. Then, 5.1 g sodium nitrate was added to the first beaker, and the mixture was stirred in water bath at 80 °C for 2 h. In the other two beakers, 1.7 g and 0.08 g of $NaNO_3$ were added, and the mixtures were stirred at room temperature for 30 and 10 min, respectively. Afterward, the samples underwent filtration, washing, drying, and roasting following the same procedure as that for Cu-ZSM-5. The mass percentages of Na were determined by XRF, and the three prepared samples were named Na1.1-ZSM-5, Na0.6-ZSM-5, and Na0.3-ZSM-5, respectively.

2.3. Back-exchange experiment

5 g Cu1.9-ZSM-5 sample was subjected to two consecutive ion-exchange treatments with 0.5 M $NaNO_3$ solutions at 80 °C for 4 h each, in a water bath. After filtration, washing, and drying, the Cu content in the zeolite was reduced to below 0.01 wt%, as measured by XRF.

2.4. Catalyst characterization

XRF analysis was used to measure the silicon-to-aluminum ratio of the samples, as well as the contents of copper and sodium. The structural characteristics of samples were characterized by scanning electron microscope (SEM), X-ray diffraction (XRD), the Brunauer-Emmett-Teller (BET) method with nitrogen adsorption-Brunauer-Emmett-Teller (N_2-BET), and ^{27}Al and ^{29}Si magic angle spinning nuclear magnetic resonance (MAS NMR). The acidity of catalysts was analyzed by Fourier transform infrared (FTIR), pyridine adsorption FTIR spectra, and ^{1}H MAS NMR. The state of copper was investigated by high-angle annular dark field scanning transmission electron microscopy (HAADF-STEM), energy dispersive X-ray spectroscopy (EDS) elemental mapping, Cu *K*-edge X-ray absorption spectroscopy (XAS), ultraviolet-visible (UV-vis) diffuse-reflectance spectra, and electron paramagnetic resonance (EPR). More detailed description of the characterization processes can be found in the Supporting Information.

2.5. In-situ FTIR measurements of NO adsorption

In-situ FTIR spectra of nitric oxide (NO) adsorbed were recorded on a Thermo Nicolet iS50 FTIR spectrometer equipped with a mercury cadmium telluride (MCT) detector and operando cell with a CaF_2 window. Optical adsorption was measured from 400 to 4000 cm^{-1} with a resolution of 4 cm^{-1} optical resolution and 128 scans. Spectra of surface species were obtained by subtraction of the pre-treated Cu-ZSM-5 spectrum before the reaction. 20 mg Cu-ZSM-5 was pressed in a self-supporting disc and loaded into the sample cell. Before the measurements, the samples were activated in the IR cell attached to a vacuum line at 723 K for 1 h. A low-temperature vacuum cell cooled with liquid nitrogen was used for NO adsorption measurements. The gases were introduced into the cell and the spectra were collected immediately. Different

spectra were obtained by the subtraction of the spectra of the activated samples from the spectra of samples with the adsorbate. For the change of atmospheric experiments, three sets of spectra were obtained: (1) spectra of NO adsorbed over the fresh Cu-ZSM-5; (2) spectra of NO adsorbed over Cu-ZSM-5 after the oxidation in O_2, and (3) spectra of NO adsorbed over Cu-ZSM-5 after oxidation with O_2 and reduction in N_2. Oxidation with O_2 was carried out in situ in the vacuum IR cell. Temperature was 723 K and the oxidation time was 1 h. After the oxidation, the sample was evacuated and cooled down with liquid nitrogen, and NO was gradually adsorbed. For reduction in N_2 after the oxidation in O_2, the sample was reduced with N_2 at 723 K for 2 h followed by evacuation. Then, the sample was cooled down and probe molecules were adsorbed at liquid nitrogen temperature.

For the in-situ coupling reaction of cyclohexane and CO_2, four sets of spectra were obtained: (1) spectra of NO adsorbed over O_2-activated Cu-ZSM-5 sample; (2) spectra of NO adsorbed over Cu-ZSM-5 after the reaction with cyclohexane; (3) spectra of NO adsorbed over Cu-ZSM-5 after the reaction with cyclohexane and reactivated in CO_2; and (4) spectra of NO adsorbed over Cu-ZSM-5 after the reaction with cyclohexane and CO_2. Activation in O_2 was conducted in a vacuum IR cell at 723 K for 1 h, after which the sample was evacuated. Then, cyclohexane was introduced into the IR cell along with nitrogen at 798 K for 10 min. After the reaction, the sample was cooled down with liquid nitrogen and NO was gradually adsorbed. For the reaction with CO_2 after the reaction with cyclohexane, the sample was reached with CO_2 at 723 K for 1 h followed by evacuation. Then, the sample was cooled down and probe molecules were adsorbed at liquid nitrogen temperature. Additionally, a separate experiment was performed where cyclohexane and CO_2 were simultaneously introduced into the IR cell at 798 K for 10 min. After the reaction, the sample was cooled down with liquid nitrogen, and probe molecules were adsorbed for further analysis.

2.6. Catalytic performance evaluation

The details of catalytic performance evaluation were given in the Supporting Information.

3. Results and discussion

3.1. Structure characterization

Cu-ZSM-5 samples with varying Cu contents (Table S1) were synthesized to investigate the relationship between the nature of Cu species and catalytic performance. SEM (Fig. S1) coupled with N_2 BET (Fig. S2) analysis indicates that all samples exhibit comparable morphologies and N_2 adsorption-desorption isotherms, and analogous diffraction peaks are observed in XRD (Fig. S3), suggesting that the crystal and pore structure of ZSM-5 samples remained intact following Cu ion-exchange. The influence of Cu loading on the ZSM-5 framework was further examined using ^{27}Al and ^{29}Si MAS NMR (Figs. S4 and S5). The observation of similar peak shapes in the NMR spectra indicates that the introduction of Cu did not exert a discernible influence on the framework structure of zeolites.

3.2. Catalytic performance analyses

Fig. S6 illustrates the aromatization performance of industrial naphtha (composition detailed in Table S2) over H-ZSM-5 and Cu1.9-ZSM-5 catalysts. The introduction of Cu species significantly enhances aromatics selectivity, particularly for benzene, toluene, and xylene (BTX). Cyclohexane was chosen as a model substrate to explore the relationship between Cu species and catalytic activity [36,37]. Compared to H-ZSM-5, Cu-ZSM-5 catalysts exhibit higher aromatics selectivity, which increases with the increase of Cu content or reaction temperature, as illustrated in Fig. 1(a–c). Specifically, the aromatics selectivity of Cu2.4-ZSM-5 was improved by 30.97% compared to H-ZSM-5 at 575 °C. Meanwhile, similar trends are observed in the aromatization of *n*-hexane, as shown in Fig. S7, underscoring the strong aromatization capacity of Cu-ZSM-5 catalysts, especially at elevated temperatures.

3.3. Influence of Brønsted acid sites

Aromatics formation from cyclohexane over Cu-ZSM-5 catalysts occurs via two pathways: (i) the hydrogen transfer reaction on Brønsted acid sites (BASs) and (ii) the dehydrogenation reaction facilitated by Cu species [38,39]. FTIR analysis of the characteristic Si(OH)Al band at 3607 cm^{-1} (Fig. 1d) reveals a decrease in the amount of BASs with increasing Cu loading, indicating that Cu species replace H^+ ions in cationic positions of H-ZSM-5 sample. This reduction is further supported by the diminishing 3.9 ppm signal in the ^{1}H MAS NMR spectra (Fig. S8) and the attenuation of the 1545 cm^{-1} BAS vibrational band in pyridine-adsorbed FTIR spectra (Fig. S9), with the acid content quantified from the py-IR summarized in Table S3 [40,41].

To isolate the effect of BASs on aromatics selectivity, Na cations—catalytically inactive species—were introduced into H-ZSM-5 zeolites through a conventional ion exchange approach. The FTIR spectroscopy (Fig. 1e) and py-IR spectra (Fig. S10 and Table S4) reveal the gradual decrease in the number of BASs with the increasing Na contents, accompanied by a corresponding decline in aromatics selectivity during the reaction of cyclohexane conversion (Fig. 1f). These findings confirm that the enhanced aromatics selectivity in Cu-ZSM-5 is not related to changes in BAS density but rather to the activity of Cu species.

3.4. State of copper species

The structural states of Cu active sites within the Cu1.9-ZSM-5 sample were investigated by comparing HAADF-STEM images, EDS elemental maps, and Cu *K*-edge X-ray absorption near-edge structure (XANES) spectroscopy. EDS mapping results (Fig. 2a) show a uniform Cu metals distribution throughout the Cu1.9-ZSM-5 particle. No clusters are visible in the HAADF-STEM image of this sample at lower voltage (Fig. 2b). However, upon applying higher voltage, highly dispersive single Cu atoms are observed after the zeolite framework is destroyed by the electron beam (Fig. 2c), indicating that monodispersed Cu ions are the predominant copper species in Cu-ZSM-5. Besides, back-exchange experiment indicates that virtually all the Cu species were removable through ion exchange, which also confirms that the Cu present in the sample exists as truly exchanged Cu ions rather than as aggregated CuO_x species. Cu *K*-edge XANES analysis (Fig. 2d) indicates a Cu valence state of approximately +2. Cu *K*-edge Extended X-ray absorption fine structure (EXAFS) models of the Cu1.9-ZSM-5 sample used O as the nearest neighbor, with the Cu–O coordination number being refined to ~3.9 (Fig. 2e). EXAFS analysis of Cu1.9-ZSM-5, CuO, and Cu_2O shows that Cu1.9-ZSM-5 lacks the higher Z neighbors (Cu) seen in the second shell of CuO and Cu_2O. In contrast, the second shell peak of Cu1.9-ZSM-5 suggests lower Z neighbors, such as Si/Al, consistent with the formation of uniform and well-defined mononuclear Cu sites [42].

The UV-vis spectra (Fig. S11) reveal the visual signals of Cu ions, while the CuO_x species, typically observed at wavelengths near 242 nm, are not discernible [42–44]. This indicates that Cu ions are the predominant Cu species in Cu-ZSM-5. It is well established that atomically dispersed Cu^{2+} species, characterized by unpaired

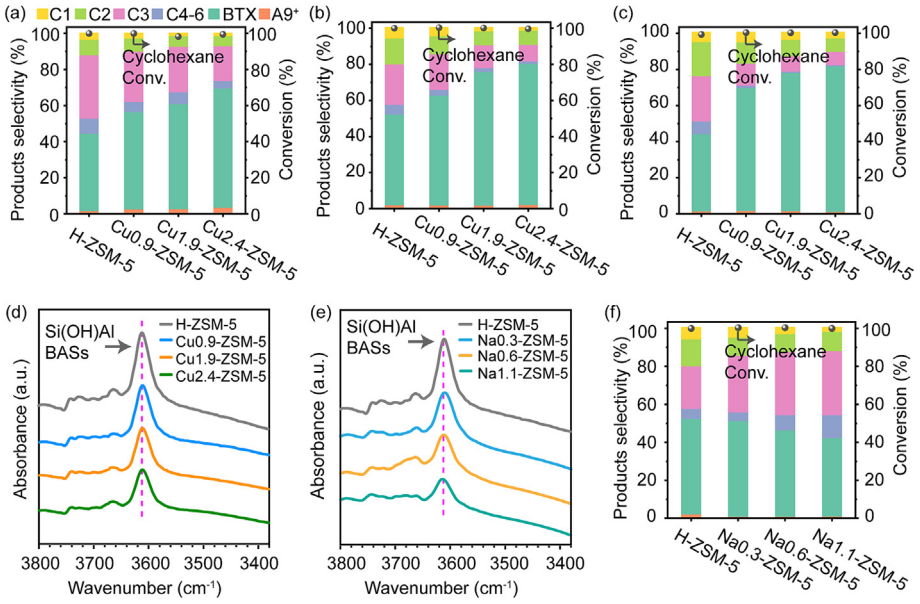

Fig. 1. Catalytic performance of cyclohexane conversion on H-ZSM-5 and Cu-ZSM-5 samples with varying reaction temperatures (a) 525 °C, (b) 575 °C, and (c) 600 °C. Reaction conditions: 0.5 g catalyst, weight hourly space velocity $(WHSV)_{cyclohexane}$ = 4 h^{-1}, He = 10 mL/min, TOS = 10 min. (d) FTIR spectra of the H-ZSM-5 and varying Cu-ZSM-5 samples. (e) FTIR spectra of the H-ZSM-5 and varying Na-ZSM-5 samples. (f) Catalytic performance of cyclohexane conversion on H-ZSM-5 and Na-ZSM-5 samples. Reaction conditions: 0.5 g catalyst, T = 575 °C, $WHSV_{cyclohexane}$ = 4 h^{-1}, He = 10 mL/min, TOS = 10 min.

electrons in the $d_{x-y}^2{}^2$ orbital, are active in EPR spectroscopy, whereas Cu^+ ions remain silent in EPR owing to the absence of an unpaired electron [45,46]. Consequently, the relative proportions of Cu^{2+} and Cu^+ species in Cu-ZSM-5 samples can be estimated by EPR (Fig. 2f), with the precise quantities of Cu species further determined by XRF (Fig. 2g); the calculated results are shown in Table S1. Approximately 60%–70% of Cu species in the Cu-ZSM-5 samples are Cu^{2+} ions, with the remainder being Cu^+. The formation of Cu^+ species in Cu-ZSM-5 results from the auto-reduction of Cu^{2+}, a phenomenon commonly observed in Cu-exchanged zeolites [23]. These sites, primarily composed of Cu^{2+} and Cu^+ ions, are critical for the observed catalytic performance. The increasing concentration of both Cu^{2+} and Cu^+ species with higher Cu loadings correlates with the enhanced aromatics selectivity during cyclohexane conversion. Here is a critical question: which Cu species predominantly drive the aromatization pathway?

3.5. Active sites

To answer the above question, FTIR spectroscopy of adsorbed nitric oxide (NO), a common probe molecule for Cu^{2+} and Cu^+ species, was employed (Fig. 3a) [25,31]. Before measurement, the Cu1.9-ZSM-5 sample was pretreated in a vacuum at 723 K for 1 h, followed by a slow introduction of NO. The spectra exhibit vibration bands at 1813, 1733, and 1825 cm^{-1}, corresponding to NO bonded to Cu^+ species, as well as 1889, 1914, and 1962 cm^{-1}, associated with various Cu^{2+} species [25,26]. These data suggest a higher quantity of Cu^+ than Cu^{2+}, inconsistent with the EPR results, likely due to further auto-reduction of Cu^{2+} species during pretreatment period. Following oxidation of the vacuum-activated Cu1.9-ZSM-5 sample with O_2 at 723 K, the FTIR spectra of adsorbed NO demonstrated a marked decrease in Cu^+ species and a concurrent increase in Cu^{2+} species. Upon subsequent reduction in N_2, low-temperature adsorbed NO on the Cu1.9-ZSM-5 sample revealed an increase in Cu^+ species and a decrease in Cu^{2+}. These findings underscore the influence of pretreatment atmosphere on the valence states of Cu species of Cu-ZSM-5.

This transformation process was further explored by in-situ EPR (Fig. 3b, c), revealing that Cu^{2+} species are converted to Cu^+ in N_2 atmosphere, while Cu^+ species are converted to Cu^{2+} in O_2 atmosphere, consistent with the FTIR spectra of adsorbed nitric oxide. Exploiting this relationship, cyclohexane conversion reactions were conducted under different pretreatment atmospheres (Fig. 3d). Compared to the un-pretreated sample, Cu1.9-ZSM-5 pretreated in N_2 atmosphere for 12 h exhibited lower aromatics selectivity, corresponding to the decreased presence of Cu^{2+} species, whereas O_2-pretreated Cu1.9-ZSM-5 showed higher aromatics selectivity due to the increased presence of Cu^{2+}. These results confirm that Cu^{2+} species serve as the more active sites for the aromatization pathway during cyclohexane conversion, though Cu^+ ions also exhibit much better aromatization performance than H^+ of the H-ZSM-5 sample.

A significant decrease in the EPR signal was observed for the spent Cu1.9-ZSM-5 sample (Fig. 3e), indicating the degradation of active Cu^{2+} species. After regeneration with air at 873 K for 4 h, the EPR signal at approximately 3300 G in the regenerated sample was comparable to that of the fresh sample, suggesting the effective recovery of Cu^{2+} species [45,47]. Furthermore, the catalytic performance of the regenerated sample was nearly identical to that of the fresh sample (Fig. 3f), further indicating the critical role of Cu^{2+} species in the cyclohexane-to-aromatics reaction. Furthermore, we also pretreated the catalyst under a hydrogen atmosphere to investigate the effect of reducing Cu^{2+}. The results, presented in Fig. S12, show that as the H_2 reduction temperature increases, the aromatics selectivity tends to decrease. This indicates that the reduction of Cu^{2+} to lower valence states (Cu^+ or Cu^0) leads to a decline in catalytic performance. This finding further confirms that Cu^{2+} is the more active site for aromatization.

3.6. Roles of carbon dioxide

Fig. 4(a and b) shows the product distribution of cyclohexane conversion on the Cu1.9-ZSM-5 sample in He and CO_2 atmospheres. Although cyclohexane was completely converted under both conditions, the introduction of CO_2 significantly enhanced

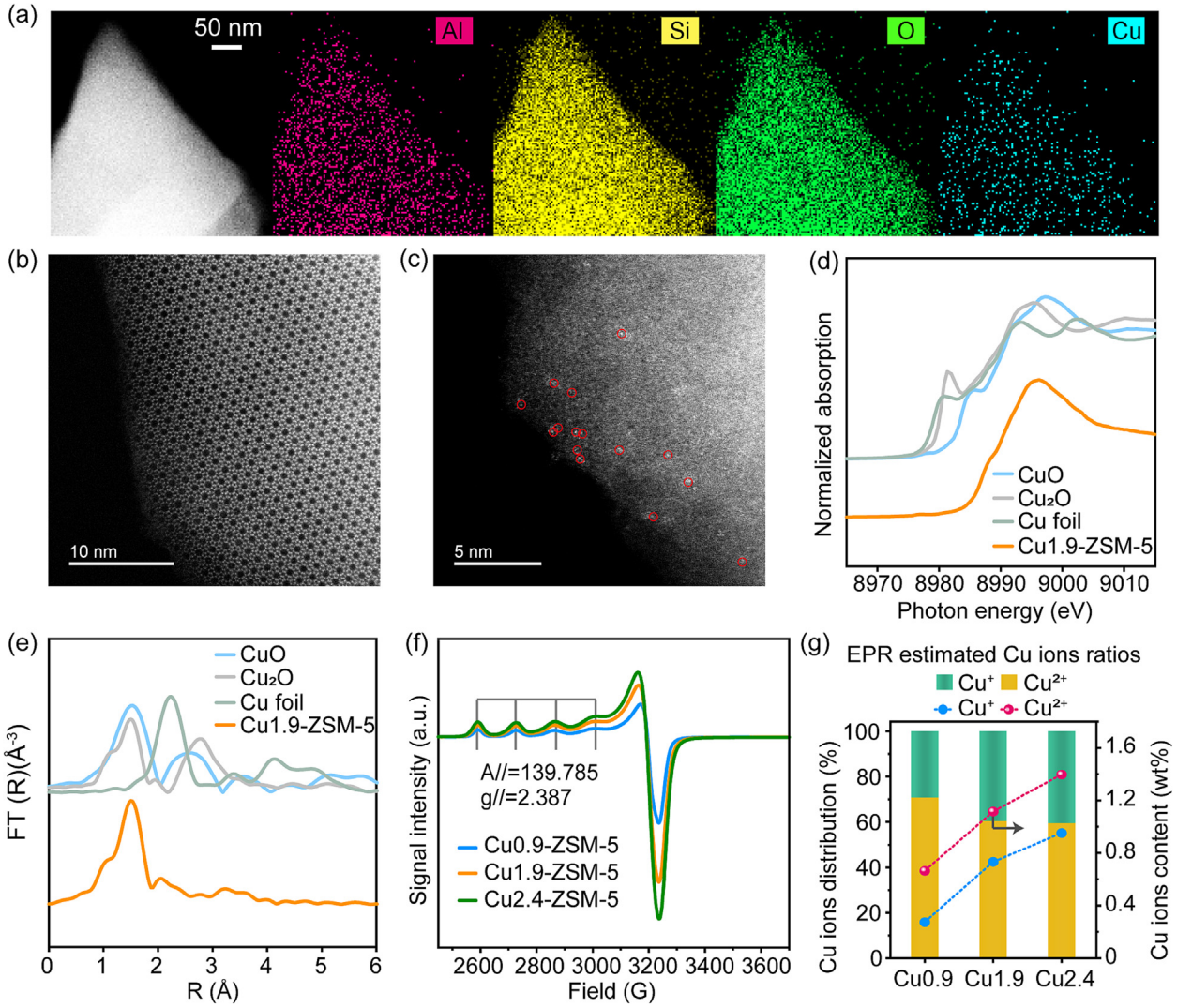

Fig. 2. (a) EDS elemental mapping of Al, Si, O, and Cu for the Cu1.9-ZSM-5 sample. HAADF-STEM images of the same area of the Cu1.9-ZSM-5 sample under (b) a lower voltage and (c) a higher voltage. (d) Cu *K*-edge spectra and (e) Fourier transform k^2-weighted EXAFS spectra of Cu foil, Cu_2O, CuO, and Cu1.9-ZSM-5 samples. (f) EPR spectra of varying Cu-ZSM-5 samples. (g) The evolution of Cu^{2+} and Cu^{+} species in Cu-ZSM-5 samples with different Cu loadings and the provided Cu content data determined using a combination of EPR and XRF.

aromatics selectivity and resulted in the formation of a substantial quantity of CO (~70% of consumed CO_2 was converted into CO). This process involves alterations in the valence state of Cu species, as monitored using FTIR of adsorbed NO (Fig. 4c) [25,31]. Before the introduction of cyclohexane, the Cu1.9-ZSM-5 sample was pretreated with O_2 at 723 K for 1 h. After interaction with cyclohexane at 798 K, FTIR spectra of NO adsorption revealed an increase in Cu^{+} content and a concurrent decrease in Cu^{2+}, indicating the reduction of Cu^{2+} species during the reaction of cyclohexane conversion. By now, the cyclohexane conversion occurs mainly under the catalytic action of Cu^{+} ions. Subsequent exposure to CO_2 resulted in the oxidation of Cu^{+} to Cu^{2+}, accompanied with the formation of CO. This transformation of Cu species explains the enhanced aromatics selectivity observed in the CO_2 atmosphere, as Cu^{2+} species are the more efficient active centers for aromatization. In addition, we have included in situ NO-IR spectra for the reaction of cyclohexane with CO_2 (Fig. S13). These spectra demonstrate that, under a CO_2 atmosphere, Cu^{2+} species are effectively stabilized. In contrast, in the absence of CO_2, the content of Cu^{+} increases while the Cu^{2+} content decreases, further supporting the role of CO_2 in stabilizing Cu^{2+}.

The above results elucidate the catalytic process occurring at the active sites of the Cu-ZSM-5 sample, which leads us to propose a reasonable mechanism. For the Cu-ZSM-5 catalyst, Cu sites catalyze the reaction of cyclohexane conversion in CO_2, and the Cu^{2+} species serve as the more efficient active sites. During the reaction, cyclohexane is converted to BTX, while the Cu^{2+} species of Cu-ZSM-5 are transformed to Cu^{+}. Upon the introduction of CO_2, the Cu^{2+} oxidation state of Cu-ZSM-5 can be stabilized during the cyclohexane aromatization reaction, which enhances the BTX selectivity.

Another striking observation is the significantly longer reaction lifetime of the Cu1.9-ZSM-5 sample in the CO_2 atmosphere (Fig. 4b). Cu1.9-ZSM-5 catalyst deactivation during cyclohexane aromatization process may arise from the formation of coke in zeolite channels. Adequate milling and granulation of spent Cu1.9-ZSM-5 increased cyclohexane conversion from 60% to 80% (Fig. S14), indicating that coke blockage partly contributed to catalyst deactivation. The coke deposition on the used Cu1.9-ZSM-5 sample during cyclohexane conversion was quantitatively analyzed using thermogravimetric analysis (TGA) under CO_2 and He atmospheres, respectively (Fig. S15). The results reveal a significantly reduced coke amount in the presence of CO_2 compared to

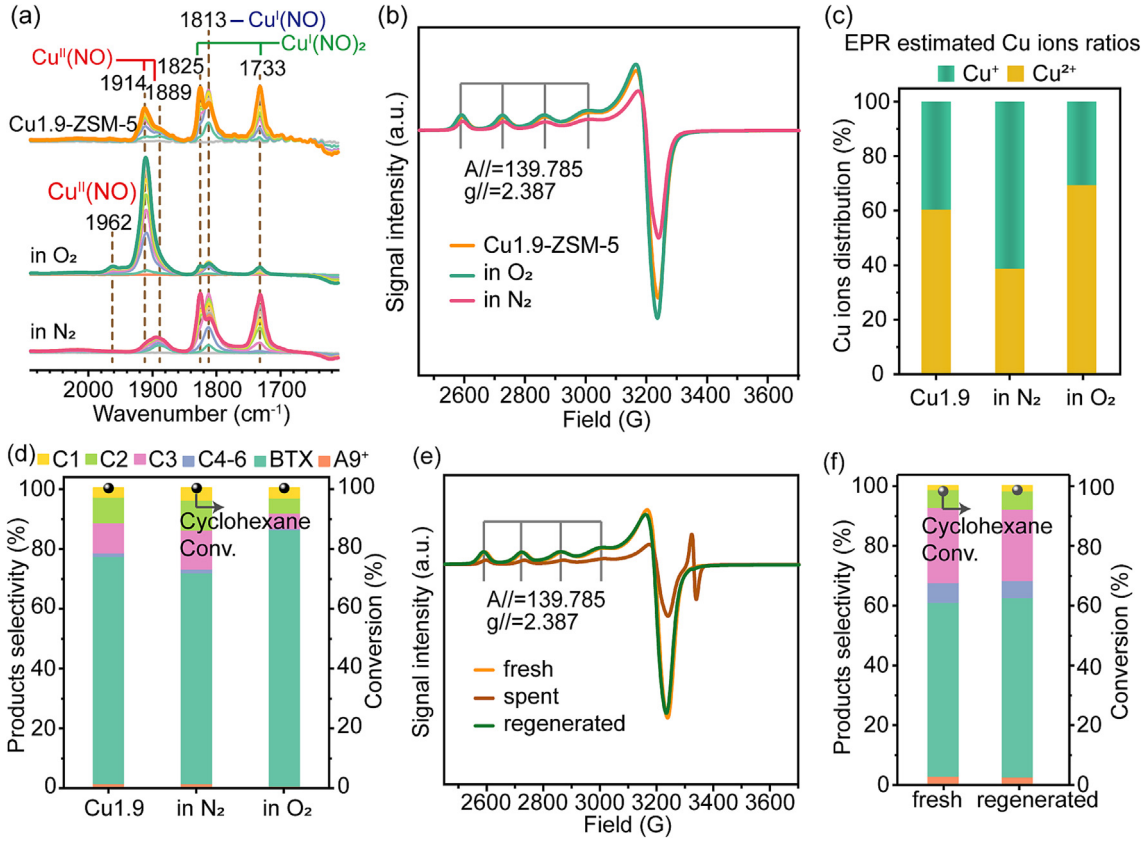

Fig. 3. (a) In-situ FTIR spectra of NO adsorbed at 100 K onto Cu1.9-ZSM-5 sample vacuum-activated (top), oxidized in O_2 (middle), and reduced in N_2 (bottom). (b) In-situ EPR spectra of the Cu1.9-ZSM-5 sample without pretreatment and pretreated in O_2 and N_2, respectively. (c) The evolution of Cu^{2+} and Cu^{+} species distribution in Cu1.9-ZSM-5 sample corresponding to the EPR data. (d) Catalytic performance of cyclohexane conversion on Cu1.9-ZSM-5 sample without being pretreated (left), with being pretreated in N_2 at 600 °C for 12 h (middle), and with being pretreated in O_2 at 600 °C for 12 h (right). Reaction conditions: 0.5 g catalyst, T = 600 °C, $WHSV_{cyclohexane}$ = 4 h^{-1}, He = 10 mL/min, TOS = 10 min. (e) EPR spectra of fresh, spent, and regenerated Cu1.9-ZSM-5 samples. (f) Catalytic performance of cyclohexane conversion on fresh (left) and regenerated (right) Cu1.9-ZSM-5 samples. Reaction conditions: 0.5 g catalyst, T = 525 °C, $WHSV_{cyclohexane}$ = 4 h^{-1}, He = 10 mL/min, TOS = 10 min.

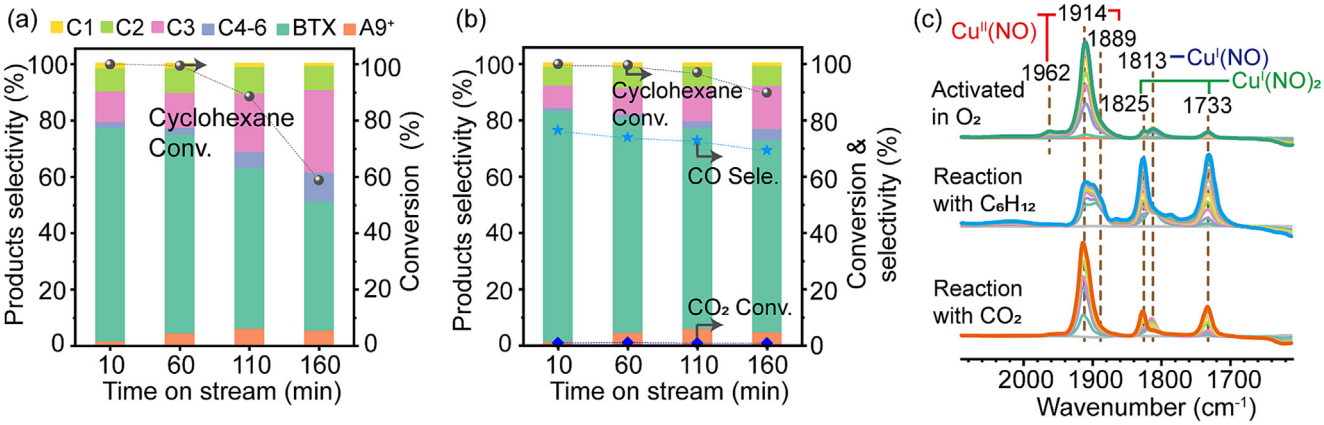

Fig. 4. Catalytic performance of cyclohexane conversion on Cu1.9-ZSM-5 sample in (a) He and (b) CO_2 plotted as a function of TOS. Reaction conditions: 0.5 g catalyst, T = 575 °C, $WHSV_{cyclohexane}$ = 4 h^{-1}, CO_2 (or He) = 43 mL/min, CO_2 (He): cyclohexane = 5:1. (c) In-situ FTIR spectra of NO adsorbed at 100 K onto Cu1.9-ZSM-5 sample that was O_2-activated (top), reacted with cyclohexane (middle), and reoxidized with CO_2 (bottom).

He, which indicates that CO_2 participates in the cyclohexane aromatization process and alters the pathway of coke formation. It has been demonstrated in our previous research [48–50] that the C of CO_2 was incorporated into the aromatic products via the oxygenated reaction intermediates, thereby balancing the H/C between alkane and aromatic, in the coupling reaction between alkane and CO_2 under high pressure condition. Moreover, CO_2 can react with the deposited carbonaceous species to eliminate coke, because the reverse Boudouard reaction (CO_2 + C → 2CO) has been shown to be feasible by thermodynamic calculations (Table S5) [51]. These effects may jointly contribute to the prolonged catalytic lifetime of Cu-ZSM-5 during the cyclohexane aromatization.

In summary, the Cu^{2+} species in Cu-ZSM-5 serve as the more efficient active sites for cyclohexane aromatization. During cyclohexane conversion, BTX products are formed, and the Cu^{2+}

species are reduced to Cu^{+} simultaneously. The introduction of CO_2 can oxidize Cu^{+} back to Cu^{2+}, which means that the active Cu^{2+} species can be stabilized relatively under the condition of co-feeding of cyclohexane and CO_2. CO_2 not only enhances aromatics selectivity but also improves the catalytic lifetime by maintaining stability of Cu active site and eliminating coke. This dual role of CO_2 represents a promising strategy for the sustainable processes of cyclohexane aromatization.

4. Conclusions

Cu-ZSM-5 zeolite exhibits exceptional performance as a catalyst for alkane aromatization, exemplified by the cyclohexane conversion reaction. In the Cu-ZSM-5 catalyst, Cu ions are the catalytically active sites for the aromatization pathway, with Cu^{2+} species identified as the more efficient aromatization centers. However, the transformation of Cu^{2+} to Cu^{+} during cyclohexane conversion leads to the reduced aromatics selectivity. The introduction of CO_2 into the reaction feed addresses the challenge by stabilizing Cu^{2+} species under reducing conditions, thereby enhancing aromatics selectivity. Additionally, CO_2 contributes to the favorable catalytic stability by suppressing coke deposition, highlighting its dual role as both a reactant and a soft oxidant. This work not only underscores the potential of Cu-ZSM-5 as a non-noble metal catalyst for alkane aromatization but also unveils an innovative role of CO_2 in the coupling reaction of alkanes and CO_2, which provides valuable insights for CO_2 utilization in catalytic processes.

Supporting information

The Supporting Information is available for this paper.

CRediT authorship contribution statement

Gaili Fan: Writing – original draft, Visualization, Validation, Investigation, Formal analysis, Data curation, Conceptualization. **Rongsheng Liu:** Writing – review & editing, Visualization, Conceptualization. **Yang Zhao:** Investigation. **Enze Chen:** Formal analysis. **Siyang Yan:** Investigation. **Jingfeng Han:** Investigation. **Jiaxu Liu:** Resources. **Zhengxi Yu:** Writing – review & editing, Supervision, Project administration. **Zhongmin Liu:** Writing – review & editing, Project administration, Funding acquisition.

Declaration of competing interest

The authors declare that they have no known competing financial interests or personal relationships that could have appeared to influence the work reported in this paper.

Acknowledgments

This work was supported by the National Natural Science Foundation of China (Grant Nos. 22288101, 22472016), the National Key Research and Development Program of the Ministry of Science and Technology (No. 2022YFE0116000), the Chinese Academy of Sciences Strategy Leading Technology Project (No. XDA29000000) and the Youth Innovation Promotion Association CAS (No. 2021182). We thank the SSRF (BL14W) beamline for experimental data collection.

Appendix A. Supplementary material

Supplementary data to this article can be found online at https://doi.org/10.1016/j.jechem.2025.02.048.

References

[1] H.A. Wittcoff, B.G. Reuben, J.S. Plotkin, Industrial organic chemicals, John Wiley & Sons, 2012.
[2] J. Pennington, Petrochemicals, an introduction to industrial chemistry, Springer, 1996, pp. 350–402.
[3] M.R. Rahimpour, M. Jafari, D. Iranshahi, Appl. Energy 109 (2013) 79–93. https://doi.org/10.1016/j.apenergy.2013.03.080.
[4] B. Valle, A. Remiro, N. García-Gómez, A.G. Gayubo, J. Bilbao, J. Chem. Technol. Biotechnol. 94 (3) (2019) 670–689. https://doi.org/10.1002/jctb.5758.
[5] D. Liu, L. Cao, G. Zhang, L. Zhao, J. Gao, C. Xu, Fuel Process. Technol. 216 (2021) 106770. https://doi.org/10.1016/j.fuproc.2021.106770.
[6] J.J. Sattler, J. Ruiz-Martinez, E. Santillan-Jimenez, B.M. Weckhuysen, Chem. Rev. 114 (20) (2014) 10613–10653. https://doi.org/10.1021/cr5002436.
[7] M. Guisnet, N.S. Gnep, Appl. Catal. A 146 (1) (1996) 33–64. https://doi.org/10.1016/0926-860x(96)00282-7.
[8] K. Cheng, L.I. van der Wal, H. Yoshida, J. Oenema, J. Harmel, Z. Zhang, G. Sunley, J. Zečević, K.P. de Jong, Angew. Chem. 132 (9) (2020) 3620–3628. https://doi.org/10.1002/ange.201915080.
[9] C.S. Triantafillidis, A.G. Vlessidis, L. Nalbandian, N.P. Evmiridis, Microporous Mesoporous Mater. 47 (2–3) (2001) 369–388. https://doi.org/10.1016/S1387-1811(01)00399-7.
[10] I. Pinilla-Herrero, E. Borfecchia, J. Holzinger, U.V. Mentzel, F. Joensen, K.A. Lomachenko, S. Bordiga, C. Lamberti, G. Berlier, U. Olsbye, J. Catal. 362 (2018) 146–163. https://doi.org/10.1016/j.jcat.2018.03.032.
[11] Q. Li, F. Zhang, J. Jarvis, P. He, M.M. Yung, A. Wang, K. Zhao, H. Song, Fuel 219 (2018) 331–339. https://doi.org/10.1016/j.fuel.2018.01.104.
[12] P. Gao, J. Xu, G. Qi, C. Wang, Q. Wang, Y. Zhao, Y. Zhang, N. Feng, X. Zhao, J. Li, ACS Catal. 8 (10) (2018) 9809–9820. https://doi.org/10.1021/acscatal.8b03076.
[13] Y. Ono, Catal. Rev. 34 (3) (1992) 179–226. https://doi.org/10.1080/01614949208020306.
[14] T. Fu, J. Shao, Z. Li, Appl. Catal. B 291 (2021) 120098. https://doi.org/10.1016/j.apcatb.2021.120098.
[15] Y. Ni, A. Sun, X. Wu, G. Hai, J. Hu, T. Li, G. Li, Microporous Mesoporous Mater. 143 (2–3) (2011) 435–442. https://doi.org/10.1016/j.micromeso.2011.03.029.
[16] K.T. Dinh, M.M. Sullivan, K. Narsimhan, P. Serna, R.J. Meyer, M. Dincă, Y. Román-Leshkov, J. Am. Chem. Soc. 141 (29) (2019) 11641–11650. https://doi.org/10.1021/jacs.9b04906.
[17] M.B. Gawande, A. Goswami, F.-X. Felpin, T. Asefa, X. Huang, R. Silva, X. Zou, R. Zboril, R.S. Varma, Chem. Rev. 116 (6) (2016) 3722–3811. https://doi.org/10.1021/acs.chemrev.5b00482.
[18] J. Gong, H. Yue, Y. Zhao, S. Zhao, L. Zhao, J. Lv, S. Wang, X. Ma, J. Am. Chem. Soc. 134 (34) (2012) 13922–13925. https://doi.org/10.1021/ja3034153.
[19] W. Wang, S. Wang, X. Ma, J. Gong, Chem. Soc. Rev. 40 (7) (2011) 3703–3727. https://doi.org/10.1039/C1CS15008A.
[20] M. Jabłońska, R. Palkovits, Appl. Catal. B 181 (2016) 332–351. https://doi.org/10.1016/j.apcatb.2015.07.017.
[21] U.R. Pillai, S. Deevi, Appl. Catal. B 64 (1–2) (2006) 146–151. https://doi.org/10.1016/j.apcatb.2005.11.005.
[22] H. Zhang, J. Lv, Z. Zhang, C. Du, S. Wang, J. Lin, S. Wan, Y. Wang, H. Xiong, ChemCatChem 14 (5) (2022) e202101609. https://doi.org/10.1002/cctc.202101609.
[23] V.L. Sushkevich, A.V. Smirnov, J.A. van Bokhoven, J. Phys. Chem. C 123 (15) (2019) 9926–9934. https://doi.org/10.1021/acs.jpcc.9b00986.
[24] A. Martini, E. Borfecchia, K. Lomachenko, I. Pankin, C. Negri, G. Berlier, P. Beato, H. Falsig, S. Bordiga, C. Lamberti, Chem. Sci. 8 (10) (2017) 6836–6851. https://doi.org/10.1039/C7SC02266B.
[25] E. Borfecchia, K. Lomachenko, F. Giordanino, H. Falsig, P. Beato, A. Soldatov, S. Bordiga, C. Lamberti, Chem. Sci. 6 (1) (2015) 548–563. https://doi.org/10.1039/C4SC02907K.
[26] F. Giordanino, P.N. Vennestrøm, L.F. Lundegaard, F.N. Stappen, S. Mossin, P. Beato, S. Bordiga, C. Lamberti, Dalton Trans. 42 (35) (2013) 12741–12761. https://doi.org/10.1039/C3DT50732G.
[27] M.H. Groothaert, J.A. van Bokhoven, A.A. Battiston, B.M. Weckhuysen, R.A. Schoonheydt, J. Am. Chem. Soc. 125 (25) (2003) 7629–7640. https://doi.org/10.1021/ja029684w.
[28] Y. Kuroda, M. Iwamoto, Top. Catal. 28 (2004) 111–118. https://doi.org/10.1023/B:TOCA.0000024340.33790.f8.
[29] D.-J. Liu, H.J. Robota, Catal. Lett. 21 (1993) 291–301. https://doi.org/10.1007/BF00769481.
[30] G. Turnes Palomino, P. Fisicaro, S. Bordiga, A. Zecchina, E. Giamello, C. Lamberti, J. Phys. Chem. B 104 (17) (2000) 4064–4073. https://doi.org/10.1021/jp993893u.
[31] V.L. Sushkevich, D. Palagin, M. Ranocchiari, J.A. van Bokhoven, Science 356 (6337) (2017) 523–527. https://doi.org/10.1126/science:aam9035.
[32] T. Kristiansen, J.A. Støvneng, M.-A. Einarsrud, D.G. Nicholson, K. Mathisen, J. Phys. Chem. C 116 (38) (2012) 20368–20379. https://doi.org/10.1021/jp305549j.
[33] T. Kristiansen, K. Mathisen, M.-A. Einarsrud, M. Bjørgen, D.G. Nicholson, J. Phys. Chem. C 115 (39) (2011) 19260–19268. https://doi.org/10.1021/jp2058782.
[34] X. Jin, J. Ding, Q. Xia, G. Zhang, C. Yang, J. Shen, B. Subramaniam, R.V. Chaudhari, J. CO_2 Util. 34 (2019) 115–148. https://doi.org/10.1016/j.jcou.2019.05.024.
[35] T. Sakakura, J.-C. Choi, H. Yasuda, Chem. Rev. 107 (6) (2007) 2365–2387. https://doi.org/10.1021/cr068357u.

[36] A.D. Klerk, Industrial Arene Chemistry: Markets, Technologies, Sustainable Processes and Cases Studies of Aromatic Commodities 1 (2023) 111–143. doi: 10.1002/9783527827992.ch5.
[37] S.L. Nauert, L. Savereide, J.M. Notestein, ACS Catal. 8 (8) (2018) 7598–7607. https://doi.org/10.1021/acscatal.8b00935.
[38] D. Gao, Y. Zhi, L. Cao, L. Zhao, J. Gao, C. Xu, M. Ma, P. Hao, Chin. J. Chem. Eng. 43 (2022) 124–134. https://doi.org/10.1016/j.cjche.2022.01.005.
[39] M. Raad, A. Astafan, S. Hamieh, J. Toufaily, T. Hamieh, J. Comparot, C. Canaff, T. Daou, J. Patarin, L. Pinard, J. Catal. 365 (2018) 376–390. https://doi.org/10.1016/j.jcat.2018.06.029.
[40] X. Sun, R. Liu, G. Fan, Y. Liu, F. Ye, Z. Yu, Z. Liu, Chin. J. Catal. 61 (2024) 154–163. https://doi.org/10.1016/S1872-2067(24)60036-7.
[41] R. Liu, B. Fan, W. Zhang, L. Wang, L. Qi, Y. Wang, S. Xu, Z. Yu, Y. Wei, Z. Liu, Angew. Chem. Int. Ed. 61 (2022) e202116990. https://doi.org/10.1002/anie.202116990.
[42] S.C. Purdy, G. Collinge, J. Zhang, S.N. Borate, K.A. Unocic, Q. Wu, E.C. Wegener, A.J. Kropf, N.R. Samad, S.F. Yuk, D. Zhang, S. Habas, T.R. Krause, J.W. Harris, M.-S. Lee, V.-A. Glezakou, R. Rousseau, A.D. Sutton, Z. Li, J. Am. Chem. Soc. 146 (2024) 8280–8297. https://doi.org/10.1021/jacs.3c13302.
[43] R. Xu, N. Liu, C. Dai, Y. Li, J. Zhang, B. Wu, G. Yu, B. Chen, Angew. Chem. Int. Ed. 60 (30) (2021) 16634–16640. https://doi.org/10.1002/anie.202105167.
[44] P. Vanelderen, B.E. Snyder, M.-L. Tsai, R.G. Hadt, J. Vancauwenbergh, O. Coussens, R.A. Schoonheydt, B.F. Sels, E.I. Solomon, J. Am. Chem. Soc. 137 (19) (2015) 6383–6392. https://doi.org/10.1021/jacs.5b02817.
[45] Y. Fan, R. Li, B. Wang, X. Feng, X. Du, C. Liu, F. Wang, C. Liu, C. Dong, Y. Ning, R. Mu, Q. Fu, Nat. Commun. 15 (1) (2024) 3046. https://doi.org/10.1038/s41467-024-47397-z.
[46] F. Gao, E.D. Walter, E.M. Karp, J. Luo, R.G. Tonkyn, J.H. Kwak, J. Szanyi, C.H.F. Peden, J. Catal. 300 (2013) 20–29. https://doi.org/10.1016/j.jcat.2012.12.020.
[47] Y. Chai, B. Qin, B. Li, W. Dai, G. Wu, N. Guan, L. Li, Natl. Sci. Rev. 10 (2023) nwad043. https://doi.org/10.1093/nsr/nwad043.
[48] C. Wei, W. Zhang, K. Yang, X. Bai, S. Xu, J. Li, Z. Liu, Chin. J. Catal. 47 (2023) 138–149. https://doi.org/10.1016/S1872-2067(23)64416-X.
[49] K. Yang, J. Li, C. Wei, Z. Zhao, Z. Liu, ACS Catal. 13 (15) (2023) 10405–10417. https://doi.org/10.1021/acscatal.3c02158.
[50] X. Ren, Z. Hu, J. Han, Y. Wei, Z. Liu, Front. Chem. Sci. Eng. 17 (11) (2023) 1801–1808. https://doi.org/10.1007/s11705-023-2325-9.
[51] E. Gomez, X. Nie, J.H. Lee, Z. Xie, J. Chen, J. Am. Chem. Soc. 141 (44) (2019) 17771–17782. https://doi.org/10.1021/jacs.9b08538.